Microsecond gamma-ray bursts produced by primordial black hole evaporation

Masaki Mori

ICRR CANGAROO Seminar, Nov. 15, 2002

Hawking radiation

- Pair creation

$$eE\lambda \geq 2mc^2$$

- Energy $(\lambda = R_{Schwalzschild} = 2GM/c^2)$

$$E = kT \propto pc \propto \frac{\hbar c}{\lambda} \propto \frac{\hbar c^3}{2GM}$$

- Luminosity

$$L \equiv \frac{dM}{dt} = (4\pi\lambda^2)(aT^4) \propto M^{-2}$$

- Time scale

$$t = \frac{M}{dM/dt} \propto M^{-3}$$

- Order estimate

$$T \approx 100\,\mathrm{MeV}\left(\frac{10^{15}\,g}{M}\right)$$

$$L \approx 10^{20}\,\mathrm{erg\,s^{-1}}\left(\frac{10^{15}\,g}{M}\right)^{-2}$$

$$t \approx 10^{10}\,\mathrm{yr}\left(\frac{10^{15}\,g}{M}\right)^{3}$$

Halzen et al. Nature 353, 807 (1991)

Evaporation of primordial black holes

- Hawking radiation (1974): black holes of masses >5×10^{14}g would be evaporating now!
- Signature: extremely short bursts of gamma-rays of duration
- Depends on particle physics:
  $dM/dt = -\alpha(M)/M^2$
  $\alpha(M)$: degrees of freedom
- Hagedorn picture: 10^{-7}s, 250MeV, 10^{34}erg
- Standard model: up to 1s, 10TeV

Halzen et al. Nature 353, 807 (1991)

Degrees of freedom

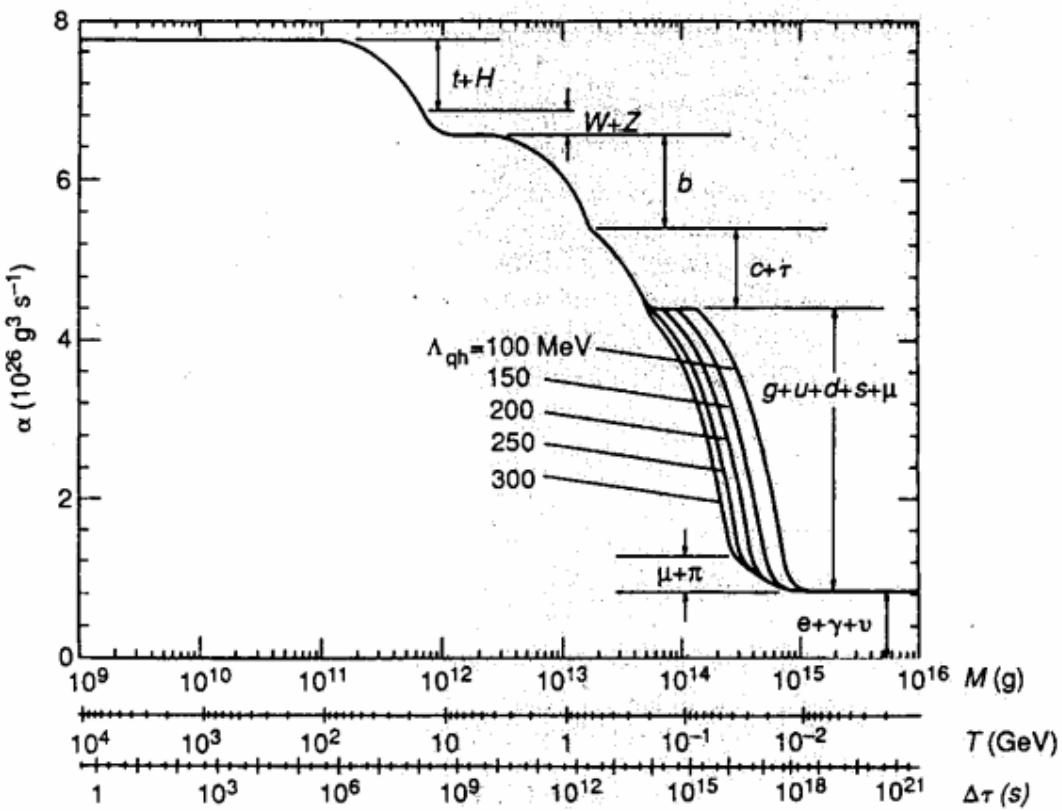

FIG. 1 The parameter α counting the degrees of freedom of the Hawking mass radiation as a function of the black-hole temperature and lifetime. Λ_{qh} is the quark–hadron deconfinement scale. The contribution from each particle species is indicated.

Halzen et al. Nature 353, 807 (1991)

Particle fluxes by a black hole

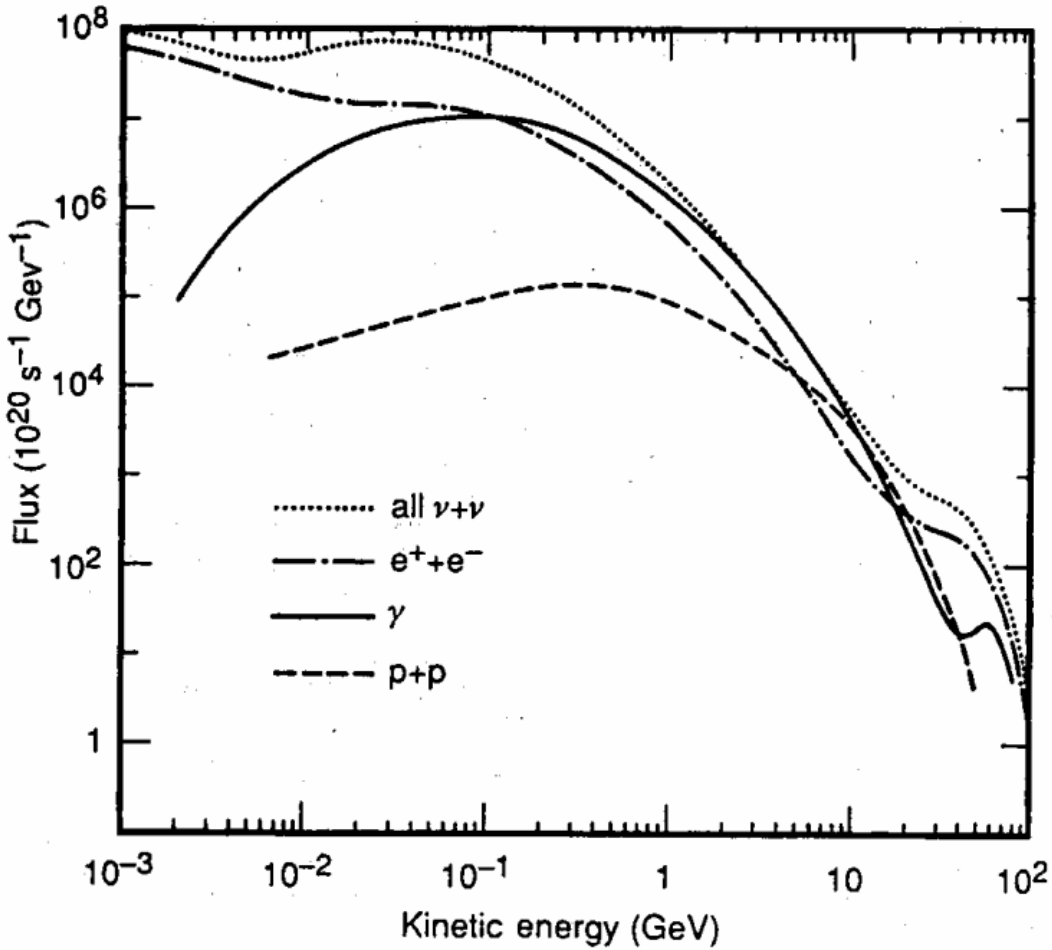

FIG. 2 Particle fluxes radiated by a black hole of temperature $T = 10$ GeV.

Halzen et al. Nature 353, 807 (1991)

Diffuse photon flux by a distribution of black holes

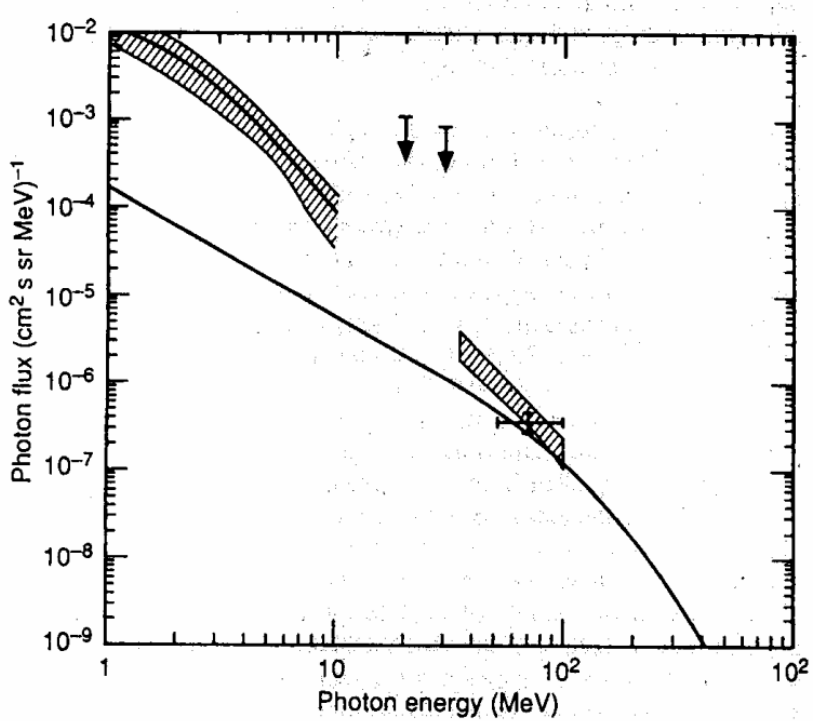

FIG. 3 Diffuse photon flux from Hawking radiation by a distribution of black holes. Shown as a solid line is the calculation for the black-hole density $\Omega_{pbh}=7.6\times10^{-9}$ leading to the bound in equation (10). Any concentration in excess of this limit would exceed the observed diffuse γ-ray background. Data and upper limits from ref. 28. The hatched areas correspond to 1σ errors.

Halzen et al. Nature 353, 807 (1991)

PBH scales vs distance

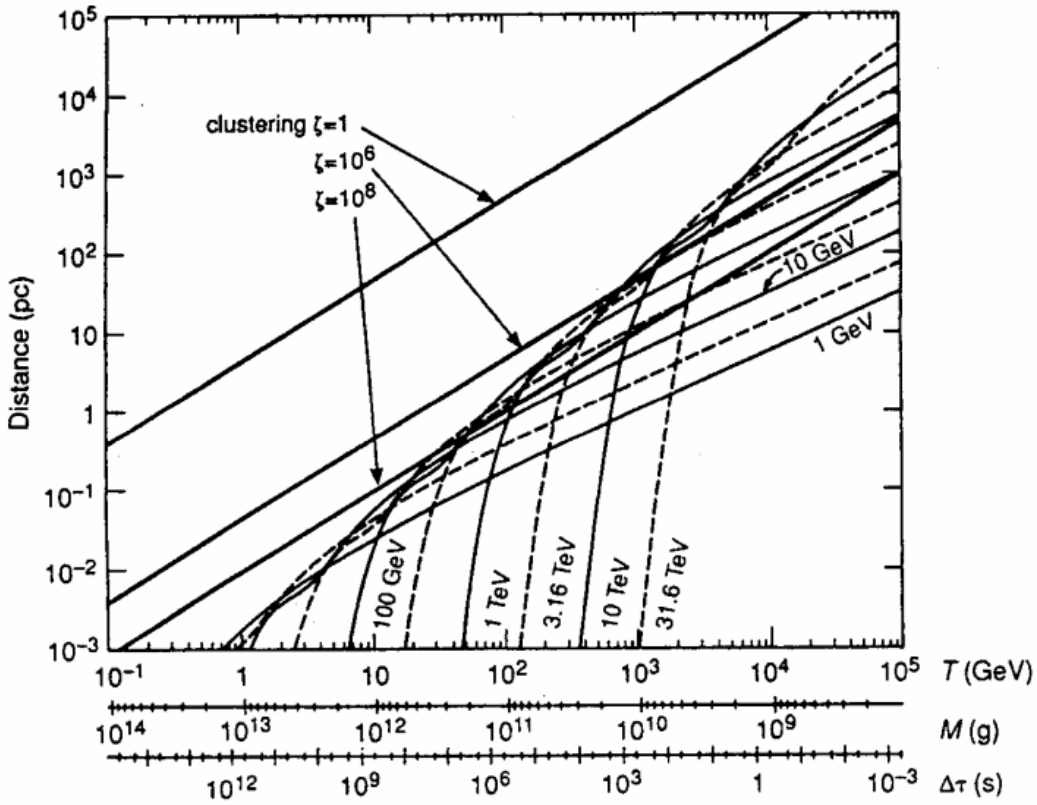

FIG. 4 The three straight lines show the distance at which the closest black hole of temperature $> T$ is expected assuming the maximum density allowed by the bound in Fig. 3. The result is shown for three values of the clustering factor ζ. The other lines show the distance at which the flux from such black hole can be resolved from the diffuse background. Detectors are assumed to have an angular resolution $\omega_D = 10^{-3}$ sr and the energy thresholds shown. The MeV bound in Fig. 3 can be improved by a detector of a given threshold in the region where its sensitivity curve exceeds the straight line.

Halzen et al. Nature 353, 807 (1991)

EGRET upper limit

- PBH signal: Multiple gamma-ray events from a given direction (within 0.6μs delay for spark chamber trigger)
- 70 multiple events in 2.5yr data were not from the same direction.

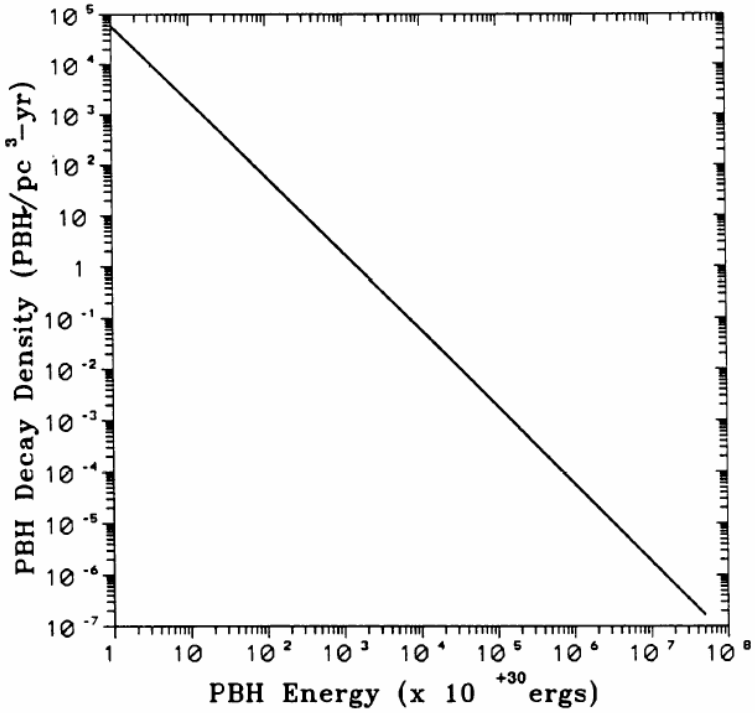

FIG. 1.—The upper limit to the primordial black hole decay density as a function of the primordial black hole energy based on the results and discussion described in the text.

Fichtel et al. ApJ 434, 557 (1994)

Evidence from BASTE data (1)

TABLE 2

CHARACTERISTICS OF SELECTED GRBs CONSISTENT WITH THE PBH EVAPORATION HYPOTHESIS

Event Characteristics	GRB Events (Selected)	Expectation for PBH Evaporation
Time duration	Time duration ~ 100 ms	In Fireball picture $\Delta\tau \approx 200$ ms.
Event hardiness in γ spectrum $H = \frac{F(115\text{–}320\ \text{KeV})}{F(55-115\ \text{KeV})}$	PHEBUS short burst data[a] have hard spectrum. Hardest γ spectrum of any GRB $\langle H \rangle \cong 6$ for BATSE (1B–3B) data	Expect hard γ spectrum, but exact value not calculable. However, in pure Hawking Process $\langle H \rangle \sim 250$.
Time history of event	Most events have simple time history: one peak	Simple time history: one peak only in event.
$\ln N$–$\ln S$ test for population spatial structure.....	BATSE 3B: corrected $\ln N$–$\ln S$ with slope $\sim -3/2$ PHEBUS short events:[b] $V/V_{max} = 0.48 \pm 0.05$	Expected $\frac{V}{V_{max}} = \frac{1}{2}$ or $\ln N - \ln S$ with a slope $= -3/2$.
Fine structure in events.....	In one BATSE event time structure of ~ 100 μs observed[c]	Fine time structure could reveal size of source.
Limit rate of GRB from PBH expected.....	$\sim 11/614$ GRB $\sim 2\%$ (1B–3B) data; Low rate	Expect low rate and $\Omega_{PBH} \sim 10^{-7}$; perhaps 10 yr.

[a] Terekhov et al. 1995.
[b] Data presented at the ESLAB-ESA conference 1995 April by J. P. Dezalay from Terekhov et al. 1995.
[c] Bhat et al. 1992.

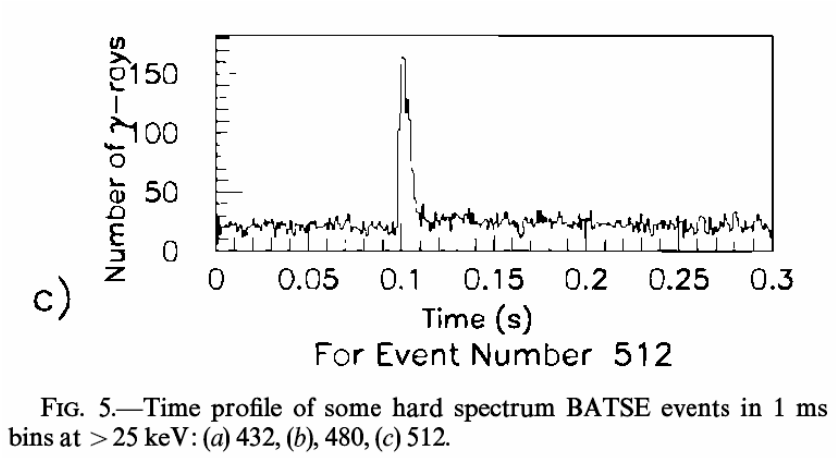

FIG. 5.—Time profile of some hard spectrum BATSE events in 1 ms bins at >25 keV: (*a*) 432, (*b*), 480, (*c*) 512.

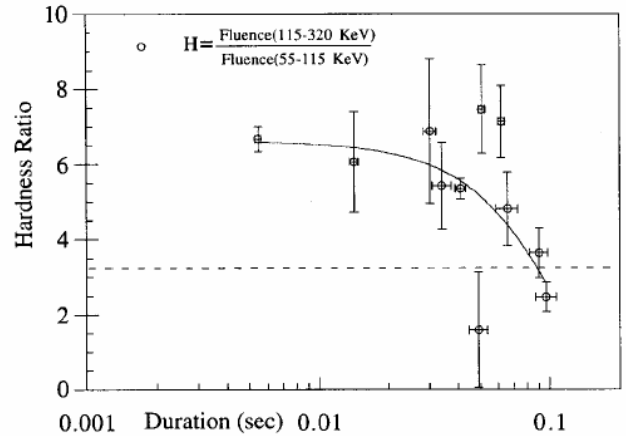

FIG. 2.—Hardness ratio for some of the γ-ray bursts reported in the BATSE 3B Catalog. A simple fitting to eq. (12) of these data indicates an anticorrelation of hardness vs. burst duration. The dashed line represents the average hardness for the bursts of time duration greater than 2. Note that these short time bursts have a much harder spectrum, a trend that would be expected if some of the short bursts came from PBH evaporation. Events have been selected with a single spike time history as would be expected for PBH evaporation.

Cline et al. ApJ 486, 169 (1997)

Evidence from BASTE data (2)

- Class of short GRBs: increasing hardness with decreasing time duration below a few 100ms.
- *"This is an interesting possibility…"*

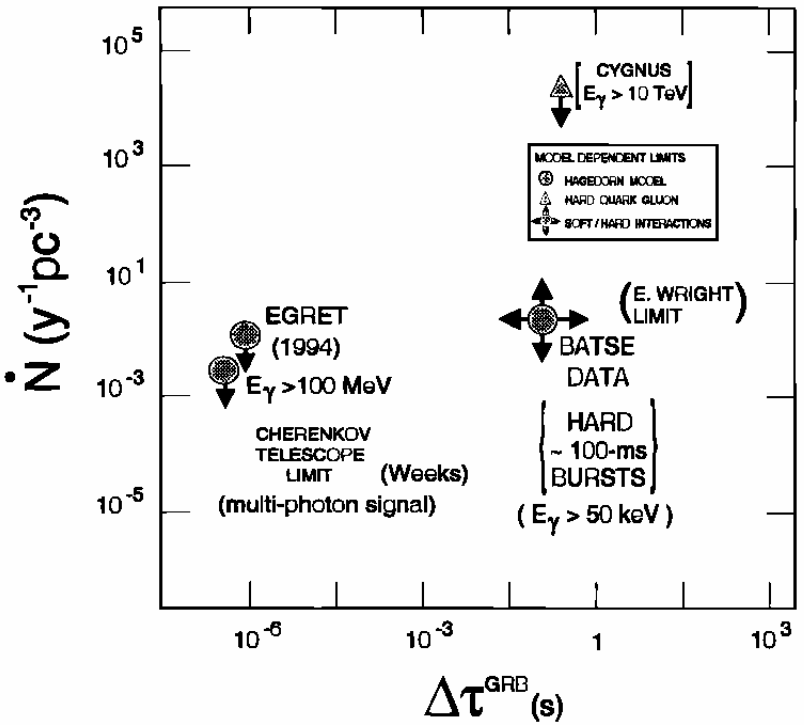

FIG. 6.—Limits for some of the PBH-GRB bursts reported in the literature (Cline 1996; Wright 1996). $\dot{N}$ refers to the limit on the number of evaporating PBHs (yr^{-1} pc^{-3}). The limits are determined by the detectors used to observe the GRB. The $\Delta\tau$ of the GRB and the model used to calculate the GRB luminosity.

Cline et al. ApJ 486, 169 (1997)

Possible detection with atmospheric Cherenkov telescopes (1)

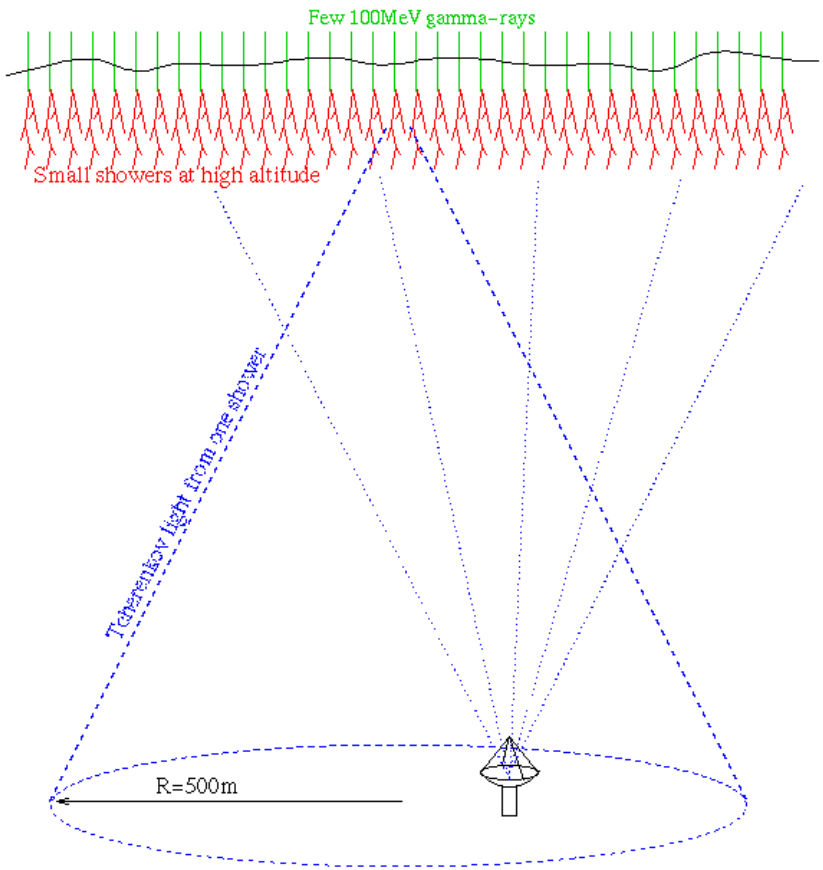

Multi-Particle Initiated Shower

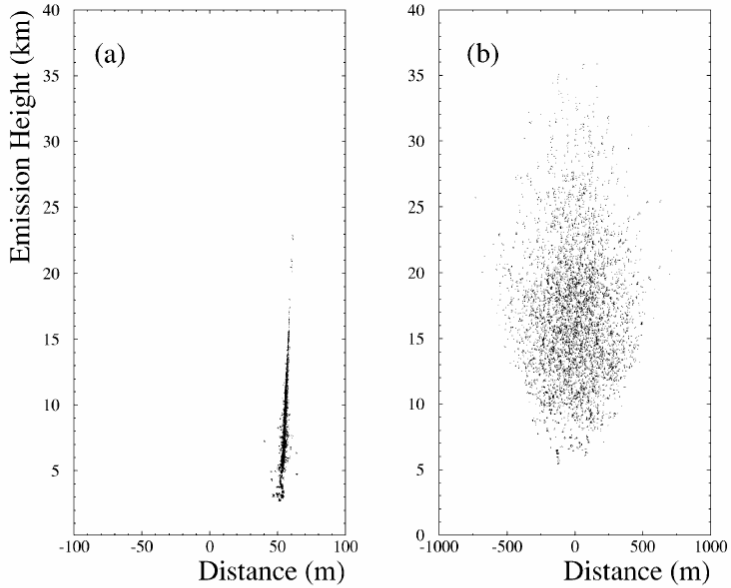

FIG. 1.—(*a*) Longitudinal and lateral distribution of the electromagnetic component of a single gamma-ray–initiated shower of 1 TeV, traced by the Cerenkov light, is shown. The dots indicate the origin of emission of individual Cerenkov photons that are detected with a Whipple-type telescope, located at an elevation of 2306 m and at *x*-coordinate zero. (*b*) We show the corresponding distribution for a multigamma-ray–initiated shower (note that lateral scale is a factor of 10 larger). The single 1 TeV gamma ray produces a narrowband Cerenkov photon distribution in the atmosphere. It can be detected up to a distance of 150 m from the shower core. For the multigamma-ray–initiated shower, Cerenkov photons that originate up to 600 m away in the lateral scale can still contribute to the Cerenkov flash detected in a telescope.

Krennrich et al. ApJ 529, 506 (2000)

Possible detection with atmospheric Cherenkov telescopes (2)

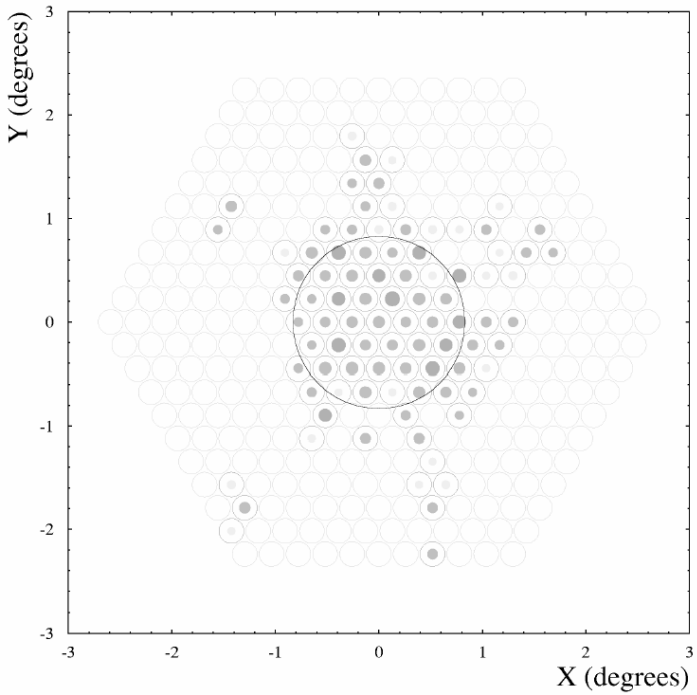

FIG. 2.—Simulated image of a burst of 300 MeV gamma rays (2.4×10^{-8} ergs cm^{-2}) arriving within 100 ns, as it would be seen with the Whipple Observatory 10 m telescope. The area and the gray scale of the filled circles indicate the relative light content in each pixel (maximum of 35 photoelectons per pixel in this event). Night-sky noise fluctuations for a 100 ns integration time are included. The image has been processed using the standard image-cleaning procedure (Reynolds et al. 1993). The circle indicates the angular extension and the shape of the image. The center of the circle coincides with the arrival direction of the burst to within 0°.1.

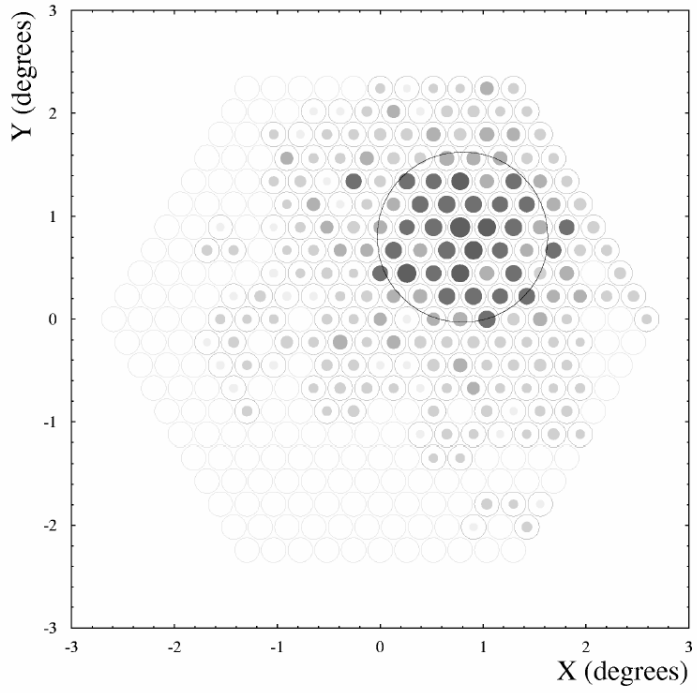

FIG. 3.—Simulated image of a burst of 300 MeV gamma rays lasting for 100 ns with a photon density of (fluence = 4.8×10^{-8} ergs cm^{-2}). The arrival direction was offset by 1°.13 from the optic axis of the telescope. Image processing using the standard image-cleaning procedure (Reynolds et al. 1993) has been applied. The circle indicates the plateau and the drop in the light density of the image where its center coincides with the arrival direction of the burst. The smooth "halo" surrounding the central image is the other characteristic feature of a burst when its light content is significantly above the night-sky noise.

Krennrich et al. ApJ 529, 506 (2000)

Possible detection with atmospheric Cherenkov telescopes (3)

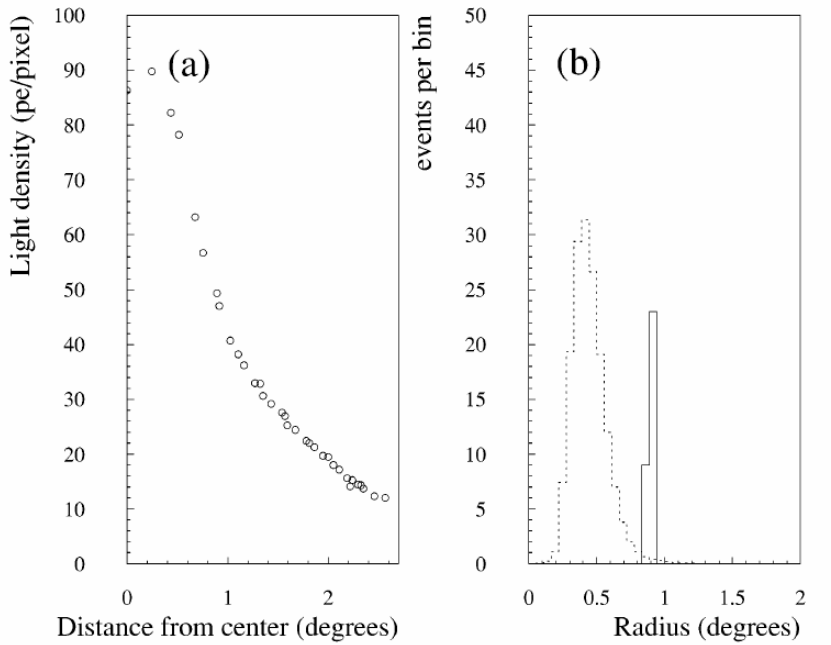

FIG. 4.—(*a*) Average radial light profile (light density vs. radial distance from image center) of wave front events is shown. (*b*) The estimated *Radius* of simulated wave front events (*solid line*) is compared with the radius of detected cosmic-ray background events (*dashed line*). Only cosmic-ray events with the same or larger light content (size) in the image as for the simulated wave front events are accepted. The average *Radius* of the images from 500 MeV bursts is approximately 0°.8, which corresponds to the half-width in the radial profile.

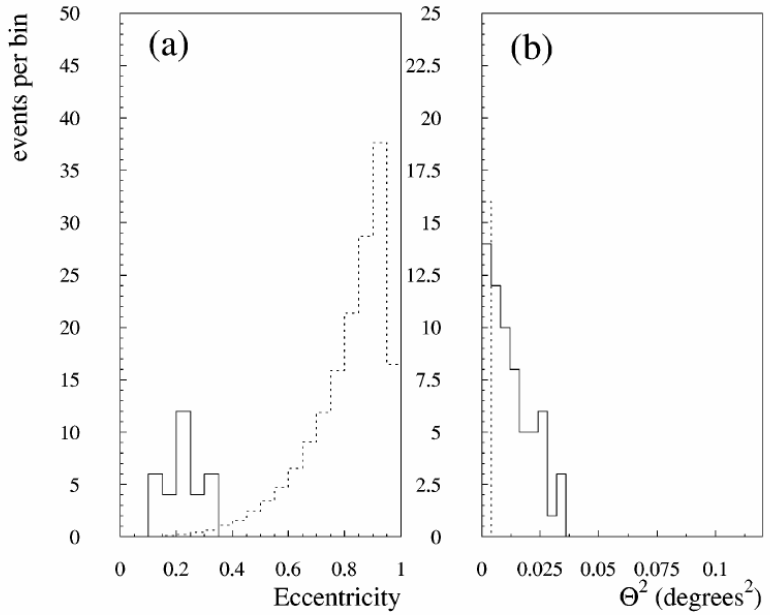

FIG. 5.—(*a*) *Eccentricity* $[(1 - \text{Width}^2/\text{Length}^2)^{1/2}]$ of images from wave front events are shown. The distribution for wave front events peaks at 0.2, as expected for almost circular images. The dotted curve represents cosmic-ray showers recorded with the Whipple Observatory 10 m telescope. (*b*) The square of the difference between the reconstructed arrival direction from the true arrival direction (Θ^2) of wave front events is plotted. The angular resolution is 0°.12 for a burst close to the detection threshold (*solid line*) and becomes 0°.06 for bursts with 4 times higher fluence values (*dotted line*). Background images from cosmic rays with isotropic arrival directions would show a flat distribution in this representation.

Krennrich et al. ApJ 529, 506 (2000)

Possible detection with atmospheric Cherenkov telescopes (4)

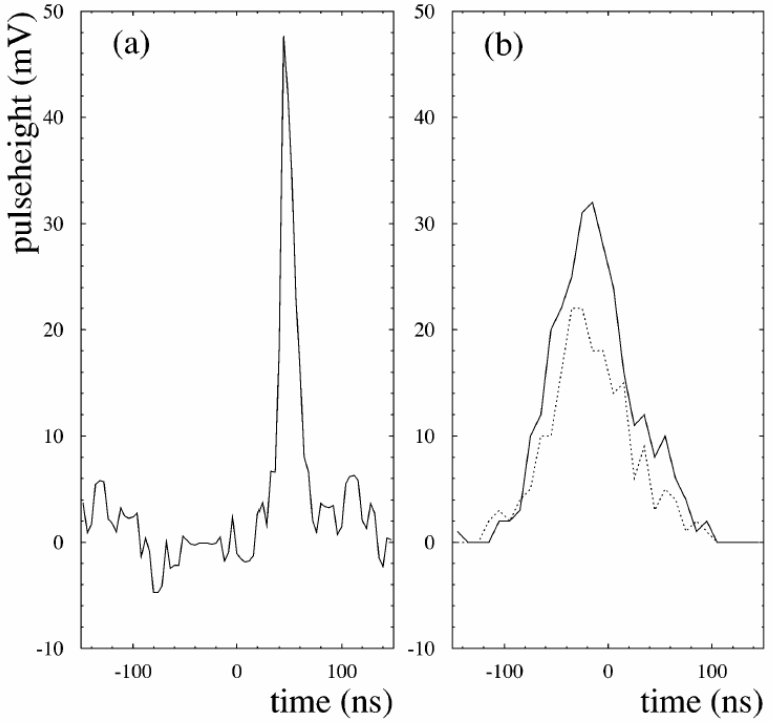

FIG. 6.—(*a*) Pulse shape for a cosmic-ray event recorded with the Whipple 10 m telescope is shown. The noise is the result of fluctuations from the night-sky background light. (*b*) The pulse profile of a simulated multiphoton-initiated cascade for two photomultipliers, one in the center of the image (*solid line*) and one by 1° off-center (*dotted line*), are shown. The burst timescale is 100 ns. Here the night-sky background noise is not included, but it would be comparable to the noise in Fig. 5*a*.

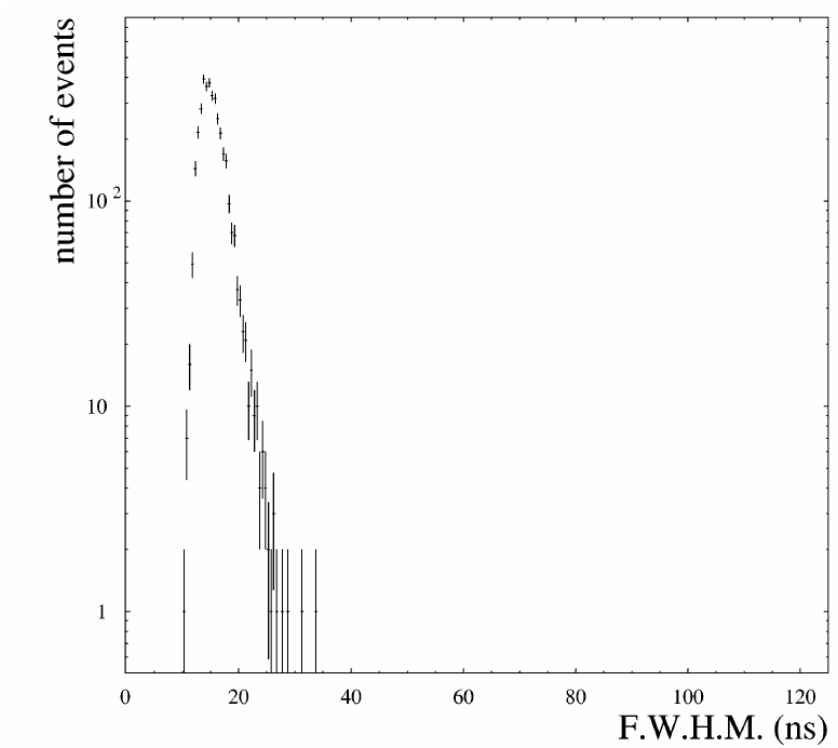

FIG. 7.—Pulse width distribution for events recorded with the Whipple 10 m telescope. The expected range for bursts from PBHs would be above 100 ns. The shortest possible pulse width from a multiphoton-initiated cascade that occurs as a result of arrival time differences between the subshowers is at about 40 ns.

Krennrich et al. ApJ 529, 506 (2000)

Possible detection with atmospheric Cherenkov telescopes (5)

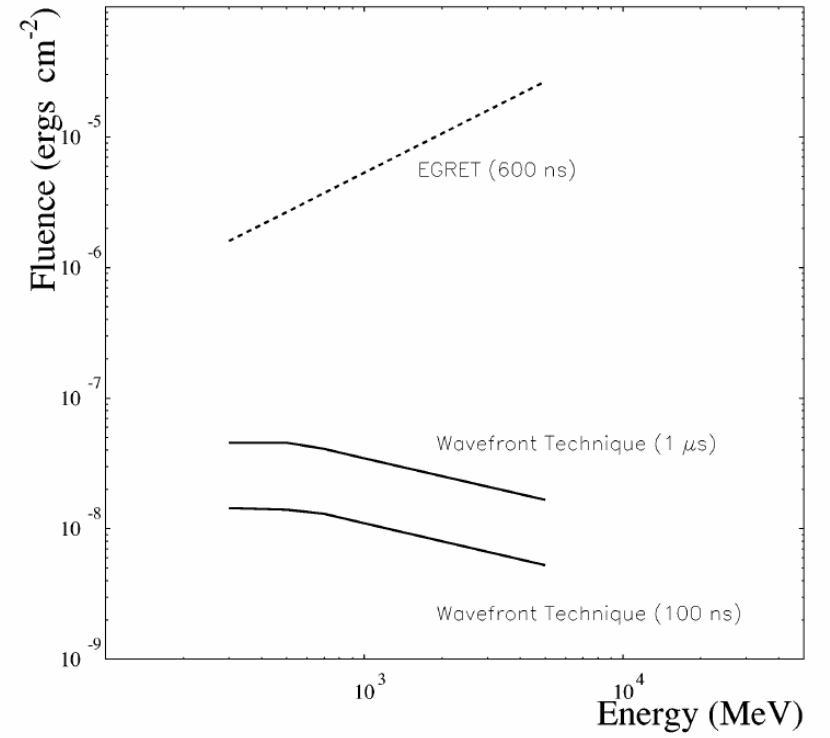

FIG. 8.—Fluence sensitivity for the wave front technique is shown as a function of energy. For comparison we also show the fluence sensitivity for EGRET, with a collection area of 0.15 m^2 in the given energy range. The detection of at least five gamma rays has been required. It can be seen that the wave front technique is about 2 orders of magnitude more sensitive than EGRET, which is mainly limited by its collection area.

Krennrich et al. ApJ 529, 506 (2000)

Short GAmma Ray Front Air Cherenkov Experiment

50MHz digitization

Bursts >50ns

Cherenkov <30ns

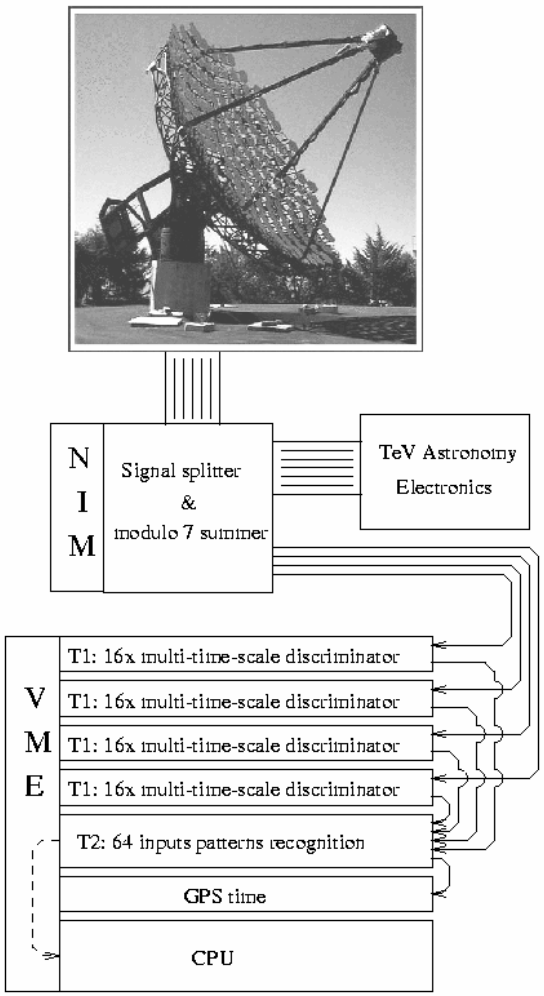

Fig. 3. General scheme of the SGARFACE experiment.

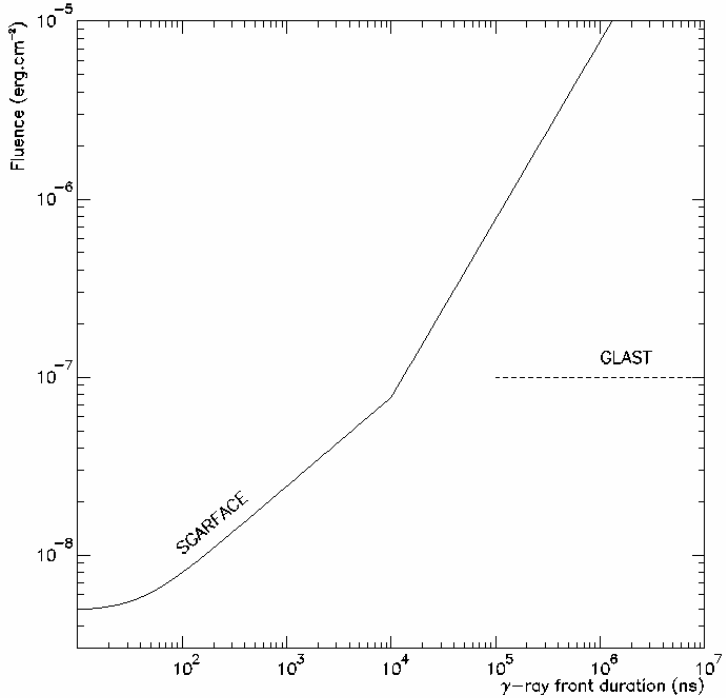

Fig. 4. The fluence sensitivity as a function of the burst duration as it should be achieved by SGARFACE is compared to the burst sensitivity of GLAST for which we assumed a minimum of 10γ-rays required for a burst to be identified.

Krennrich et al. ICRC2001 (2001)